

# IMPEDANCE OF ELECTRON BEAM VACUUM CHAMBERS FOR THE NSLS-II STORAGE RING\*

Alexei Blednykh<sup>#</sup>, Samuel Krinsky  
 BNL, NSLS-II, Upton, New York, 11973-5000, U.S.A.

## Abstract

In this paper we discuss computation of the coupling impedance of the vacuum chambers for the NSLS-II storage ring using the electromagnetic simulator GdfidL [1]. The impedance of the vacuum chambers depends on the geometric dimensions of the cross-section and height of the slot in the chamber wall. Of particular concern is the complex geometry of the infrared extraction chambers to be installed in special large-gap dipole magnets. In this case, wakefields are generated due to tapered transitions and large vertical-aperture ports with mirrors near the electron beam.

## INTRODUCTION

For a structure mirror-symmetric relative to the  $y=0$  plane but not the  $x=0$  plane, the transverse-coupling impedance for a driving bunch with transverse coordinates  $x_d, y_d$  acting on a following bunch with coordinates  $x_f, y_f$  has the form [2,3]

$$\begin{aligned} Z_x(x_d, x_f, \omega) &\equiv Z_{0x}(\omega) + x_d Z_{Dx}(\omega) + x_f Z_Q(\omega), \\ Z_y(y_d, y_f, \omega) &\equiv y_d Z_{Dy}(\omega) - y_f Z_Q(\omega) \end{aligned} \quad (1)$$

where  $Z_0$ ,  $Z_D$  and  $Z_Q$  are the monopole-, dipole- and quadrupole-impedances. Placing the following bunch on axis  $x_f = y_f = 0$ , we can express the horizontal-dipole impedance as,

$$Z_{Dx}(\omega) = [Z_x(\Delta x_d, 0, \omega) - Z_x(-\Delta x_d, 0, \omega)] / 2\Delta x_d. \quad (2)$$

It can also be evaluated via the longitudinal impedance using Nassibian and Sacherer's relation [4]

$$Z_{Dx}(\omega) = (c/\omega) [\partial^2 Z_{||}(x_d, x_f, \omega) / \partial x_d \partial x_f]_{x_d=x_f=0}. \quad (3)$$

Numerically approximating the second derivative we obtain

$$Z_{Dx}(\omega) = \frac{c}{\omega} \frac{1}{4\Delta x_d \Delta x_f} \left[ Z_{||}(\Delta x_d, \Delta x_f, \omega) - Z_{||}(\Delta x_d, -\Delta x_f, \omega) - Z_{||}(-\Delta x_d, \Delta x_f, \omega) + Z_{||}(-\Delta x_d, -\Delta x_f, \omega) \right] \quad (4)$$

The vertical-dipole impedance can be computed from

$$Z_{Dy}(\omega) = Z_y(\Delta y_d, 0, \omega) / \Delta y_d. \quad (5)$$

and it can be expressed in terms of the longitudinal impedance via

$$Z_{Dy}(\omega) = \frac{c}{\omega} \frac{1}{2\Delta y_d \Delta y_f} \times [Z_{||}(\Delta y_d, \Delta y_f, \omega) - Z_{||}(\Delta y_d, -\Delta y_f, \omega)] \quad (6)$$

In GdfidL [1] calculations, we take  $\Delta x_{d,f}$  or  $\Delta y_{d,f}$  equal to three times the grid spacing. Also, when calculating the transverse impedance in GdfidL, one cannot evaluate directly the transverse impedance on axis. Therefore, we take

$$Z_\xi(\Delta \xi_d, 0, \omega) \equiv [Z_\xi(\Delta \xi_d, \delta \xi_f, \omega) + Z_\xi(\Delta \xi_d, -\delta \xi_f, \omega)] / 2. \quad (7)$$

\*Work supported by DOE contract DE-AC02-98CH10886.

<sup>#</sup>blednykh@bnl.gov

with  $\delta \xi_f$  equal to one-half the grid spacing and  $\xi = x, y$ .

If there is mirror symmetry relative to the  $xz$ - and  $yz$ -planes, one-quarter of the structure with appropriate boundary conditions can be used for computation. For  $Z_0$  and  $Z_Q$ , magnetic boundary conditions are specified in the  $x=0$  and  $y=0$  planes. For  $Z_{Dy}$ ,  $y=0$  is electric boundary and  $x=0$  is magnetic, and the driving charge is located at  $x=0$  and  $y=\Delta y_d > 0$ . In GdfidL, the following charge cannot be located on the electric wall so one must choose  $\Delta y_f > 0$ . To avoid contributions from sextupole and higher-order modes, we have found it is better to compute  $Z_{Dy}$  using one-half of the structure ( $x > 0$ , with magnetic boundary condition on  $x=0$ ) and employ Eq. (7).

## COAXIAL PIPE AND ROUND CHAMBER

To compare GdfidL with analytic results, we consider a coaxial beam pipe with a rectangular slot in its inner conductor (Fig. 1). The radii of the inner and outer cylinders are  $a=32\text{mm}$  and  $b=42\text{mm}$ . The slot width is  $w=8\text{mm}$  and slot length  $L_{slot} \gg w$ . The thickness  $t$  of the inner wall is assumed to be as small as possible. Based on studies by Kurennoy [5], and Gluckstern and Fedotov [6,7], the longitudinal impedance for on-axis beam at low frequency can be expressed as [6]

$$\text{Im } Z_{||}(0, 0, \omega) / \omega = Z_0 0.1814 w^3 / (4\pi^2 a^2 c). \quad (8)$$

Applying Eq. (8) to the dimensions noted above, the longitudinal impedance divided by omega at low

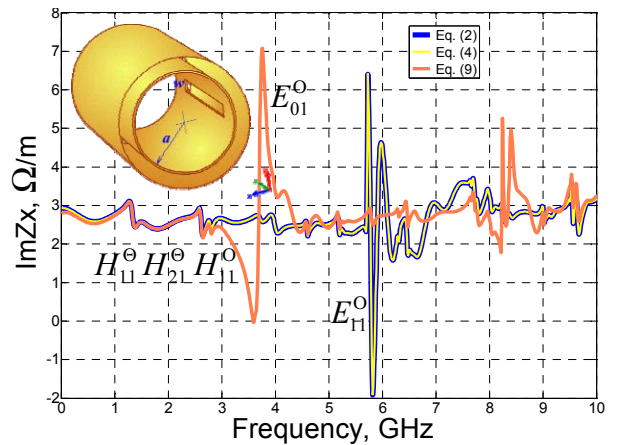


Figure 1: Imaginary part of the horizontal impedance for a coaxial pipe with a rectangular slot of  $w=8\text{mm}$  in an inner conductor with a radius  $a=32\text{mm}$ . Superscript  $\Theta$  refers to modes with dominant field between cylinders and O to modes with dominant field within inner cylinder.

frequency is  $\text{Im}Z_{\parallel}(0,0,\omega)/\omega = 0.29 \times 10^{-11}$  ( $t/a=0$ ). The longitudinal impedance, computed by GdfidL, for positions  $x=0$  and  $y=0$  of the driving and following bunches over omega is  $\text{Im}Z_{\parallel}(0,0,\omega)/\omega = 0.24 \times 10^{-11}$  ( $t/a=0.013$ ). Accordingly, the GdfidL result (for small but not vanishing thickness) is very close to the analytically calculated value.

In Fig. 1, we show the horizontal impedance as computed from Eq. (2) (blue) and Eq. (4) (yellow). There is excellent agreement. Analytic results show that for the slotted chamber the transverse impedance is related to the longitudinal impedance by

$$\text{Im}Z_{D,x}(\omega) = (4c/a^2)\text{Im}Z_{\parallel}(\omega)/\omega \quad (9)$$

Calculating the longitudinal impedance (drive and following particles on axis) by GdfidL, the result of Eq. (9) for the horizontal impedance is shown as an orange curve in Fig.1. Eq. (9) only holds for low frequency. At higher frequency, it yields a sharp resonant peak at 3.7GHz (orange line) that corresponds to the  $E_{01}^0$ -mode ( $f_c=3.6\text{GHz}$ ) as in a round waveguide (*monopole* mode). There is no such resonance in the transverse impedance. The resonant peak at frequency 5.8GHz (yellow line) of the  $\text{Im}Z_x^{Eq(2)}$  is slightly above the cutoff frequency of the  $E_{11}^0$ -mode ( $f_c=5.7\text{GHz}$ ) as in a round waveguide (*dipole* mode).

Let us compare the longitudinal impedance of the coaxial pipe having slotted inner conductor of radius  $32\text{mm}$  with that of a round slotted cylinder of radius  $32\text{mm}$  (Fig. 2). The resonance spectra differ. The two lowest resonant frequencies in the coaxial pipe correspond to the  $H_{11}^0$ -mode ( $f_c=1.29\text{GHz}$ ) and  $H_{21}^0$ -mode ( $f_c=2.58\text{GHz}$ ) with fields predominantly between the two conductors. The lowest mode that can resonate in the round chamber and also propagate inside the inner conductor of the coaxial pipe is the  $H_{11}^0$ -mode. For radius  $a=32\text{mm}$ , the  $H_{11}^0$ -mode resonates at  $2.8\text{GHz}$  in both structures. At low frequency, in the round chamber with trapezoidal port,  $\text{Im}Z_{\parallel}(0,0)/\omega = 0.16 \times 10^{-11}$ , which is a factor of 1.5 smaller than that for the coaxial pipe.

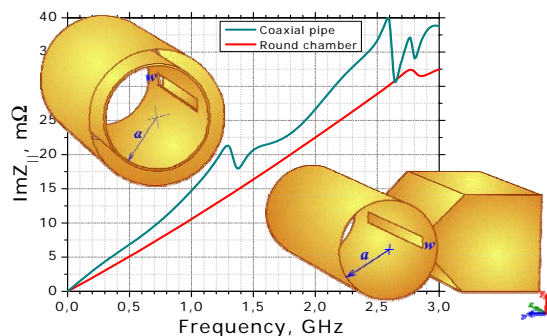


Figure 2: Imaginary part of the longitudinal impedance  $\text{Im}Z_{\parallel}(0,0,\omega)$  for a coaxial pipe with a rectangular slot in its inner conductor (dark cyan line) and for a round chamber with a rectangular slot in its wall and trapezoidal port (red line).

## ELLIPTIC VACUUM CHAMBERS

The regular electron beam vacuum chamber for the NLSLS-II storage ring has an elliptical cross-section with inner dimensions of full width  $2a=76\text{mm}$  and full height  $2b=25\text{mm}$ . According to its location in the storage ring, the design of the chamber will differ. To analyze the impedance per component we name the vacuum chambers corresponding to their location: dipole vacuum chamber (Fig. 3), quadrupole vacuum chamber (Fig. 4) and sextupole vacuum chamber (Fig. 5) [8]. In each chamber, there is a rectangular slot for extracting synchrotron radiation (SR) from the beam chamber's channel. The slot of the dipole vacuum chamber is  $15\text{mm}$  high. The slots of both the quadrupole and sextupole vacuum chambers are  $10\text{mm}$ . As Stupakov [9] demonstrated, the impedance for long slots is independent of the slot's length ( $L_{\text{slot}}$ ). Hence, for our numerical computations, the arbitrarily large slot length was taken as  $L_{\text{slot}}=80\text{mm}$ .

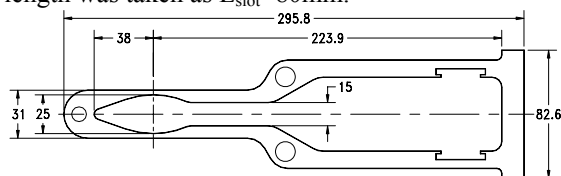


Figure 3: Dipole vacuum chamber.

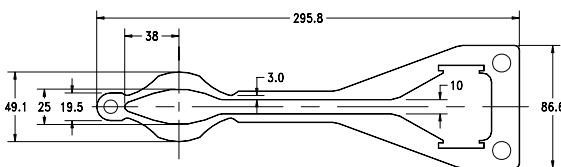


Figure 4: Quadrupole vacuum chamber.

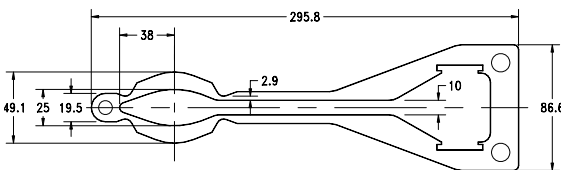


Figure 5: Sextupole vacuum chamber.

From the wakepotential and impedance functions, we calculated the horizontal kick factors ( $\kappa_x$ ) and the loss factors ( $\kappa_{\text{loss}}$ ) for a bunch length of  $\sigma_s=3\text{mm}$  rms. Table 1 presents these results and as well as the imaginary part of the horizontal impedances at low frequency ( $\text{Im}Z_x(\omega \rightarrow 0)$ ) and the longitudinal impedance divided by the harmonic number  $n=\omega/\omega_0$  at low frequency for a single component ( $(\text{Im}Z_{\parallel}/n)_0$ ), where  $\omega_0 = 2\pi \times 384.6\text{kHz}$ .

Table 1: Summary of data for the vacuum chambers.

Vacuum chambers	$\kappa_{\text{loss}}$ , V/pC	$(\text{Im}Z_{\parallel}/n)_0$ , $\Omega$	$\kappa_x$ , V/pC/m	$\text{Im}Z_x(\omega \rightarrow 0)$ , $\Omega/\text{m}$
Dipole	$3.3 \times 10^{-5}$	$0.7 \times 10^{-7}$	$4.5 \times 10^{-3}$	0.15
Quadrupole	$0.5 \times 10^{-5}$	$0.1 \times 10^{-7}$	$0.7 \times 10^{-3}$	0.02
Sextupole	$0.5 \times 10^{-5}$	$0.1 \times 10^{-7}$	$0.7 \times 10^{-3}$	0.02

## INFRARED EXTRACTION CHAMBER

Infrared (IR) extraction chambers will be installed in special large-gap dipole magnets. The extraction chambers are 2.6m long with a vertical aperture 67mm and allow the extraction of  $\sim 50\text{mrad}$  horizontal and  $\sim 25\text{mrad}$  vertical. Separation of the radiation from the electron beam is made more difficult due to the large bending radius ( $\rho=25\text{m}$ ) of the NSLS-II dipoles. Since the IR-chambers have larger vertical aperture than the regular vacuum chambers, smooth tapers are required to minimize the contribution to the longitudinal and transverse impedances. Preliminary estimates of the longitudinal and transverse impedances have been obtained using Eqs. (2) and (5) for the simplified geometries illustrated in Figure 6. The full height and the full width of the chamber are 67mm and 134mm respectively. Smooth tapered transitions, each 180mm long, are located at both ends of the structure (Fig. 6a). We modeled narrow (Fig. 6b) and trapezoid slots in x-direction (Fig. 6c), where the extraction mirror will be located.

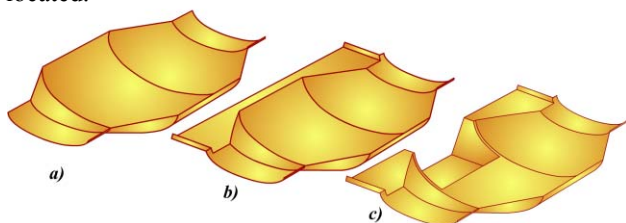


Figure 6: Simplified model of IR-extraction chamber: a) tapered elliptic chamber; b) with narrow slot; c) with trapezoidal slot.

Computations of the longitudinal wakepotential for a  $\sigma_s=3\text{mm}$  rms bunch length show that narrow and trapezoid slots do not significantly affect the short-range wakepotential and hence the loss factor. In this case tapers are the major contributors to the longitudinal broad-band impedance. For a 180mm taper length, the loss factor is  $\kappa_{loss} = 0.8 \text{ V/pC}$ . To reduce this value the taper length for the actual design geometry will be lengthened.

To direct the collected emission into the output port, the extraction mirror (copper color, 5mm thick) is first modeled at the end of the trapezoid slot, 30mm from the beam trajectory as shown in Figure 7a. However long-range wakepotential computations show that in this case resonance modes (narrow-band impedance) are generated due to the mirror which is located inside the large aperture of the chamber. The mirror is seen by the beam and generated modes are trapped in a small pocket between the tapered transition and the mirror.

To avoid generation of resonant modes inside the chamber, we studied several variants of mirror position while maintaining the required extraction angles. One of the variants was found promising. To avoid a pocket behind the mirror, we located the mirror at a point right after the widened cross-section had tapered back down to

the regular dimensions, as shown in Figure 7b. In this case, the extraction mirror is hidden behind the tapered transition. This design eliminated the problem of resonant modes due to the mirror.

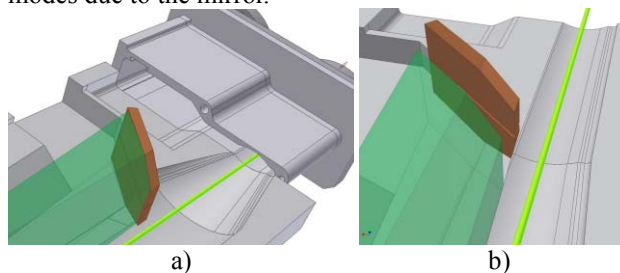


Figure 7: a) Mirror is located in front of the tapered transition. b) Mirror is located inside the regular vacuum chamber behind the tapered transition. The green line represents the electron beam and the green shaded region represents the IR radiation.

The design of the infrared beam extraction chamber for the NSLS-II storage ring is still continuing. Results of the short-range wakepotentials for a 3mm rms bunch length in a more realistic (and complex) model of the IR-extraction chamber will be presented in a future publication. A prototype chamber will be built to verify computed results by experimental measurements.

We thank Larry Carr and David Scott Coburn for collaborative work on the design of the IR chamber for NSLS-II. Also we thank D. Robin and F. Sannibale for discussion of the results of impedance studies for the IR-extraction chambers for CIRCE [10].

## REFERENCES

- [1] W. Bruns, GdfidL, <http://www.gdfidl.de>
- [2] A. Chao, S. Heifets and B. Zotter, Phys. Rev. ST-AB **5**, 111001 (2002).
- [3] S. Heifets, A. Wagner, B. Zotter, "Generalized impedances and wakes in asymmetric structures," SLAC / AP 110, January 1998.
- [4] G. Nassibian and F. Sacherer, "Methods for measuring transverse coupling impedances in circular accelerators," NIM 159 (1979) 21-27.
- [5] S. Kurennoy, "On the coupling impedance of a hole or slot," CERN SL/91-29 (AP), 1991.
- [6] A.V. Fedotov and R.L. Gluckstern, "Impedance and resonance issues for a long rectangular slot in a coaxial liner," Phys. Rev. E, V56, 6, December 1997.
- [7] R.L. Gluckstern, "Coupling impedance of a single hole in a thick-wall beam pipe," Phys. Rev. A, V46, 2, July 1992.
- [8] NSLS-II Conceptual Design Report 2006.
- [9] G. Stupakov, "Coupling impedance of a long slot and an array of slots in a circular vacuum chamber," Phys. Rev. E 51, 3515 (1995).
- [10] J.M Byrd et al., "CIRCE: a dedicated storage ring for coherent THz synchrotron radiation", Infrared Physics & Technology, 45, 2004.